Aerodynamic performance improvement using a micro-cylinder as a passive flow control around the S809 airfoil

Aerodynamic performance improvement using a micro-cylinder as a passive flow control around the S809 airfoil

W Mostafa[1,*], A Abdelsamie[2,3], MMohamed[2,4], DThévenin[3] andM. Sedrak[2].
[1]Egyptian Russian University
[2]Lab. of Fluid Mechanics, Helwan University, Cairo, Egypt
[3]Lab. of Fluid Dynamics & Technical Flows, University of Magdeburg "Otto von Guericke", Germany
[4]Mechanical Engineering Dept, College of Engineering and Islamic Architecture, Umm Al-Qura University, Makkah, Saudi Arabia
[*]Corresponding author:eng.wafaamostafa@gmail.com

Abstract. Aerodynamic performance improvement of airfoilsis the first step towards enhancement ofthe wind turbine performance in electricity generation and energy conversion inrenewable energy applications. The flow behavioraround wind turbine blades profilecan be improved by introducing active and/or passive flow controls. This work numerically describes the impact of adding micro-cylinder, as a passive flow control around S809 airfoil, on aerodynamic performance under various operating conditions. A suitable combination of flow analysis and optimization technique has been used in the current work.The numerical simulation has been performed using ANSYSFluent 18.2 software. The airfoil was numerically analysed in flow atReynolds number of 10^6; aerodynamic coefficients (lift and drag coefficients) at different angle of attacks were validated with the experimental data reported by Somers in NREL. The Response Surface Method (RSM) is applied to obtain the optimum position of micro-cylinder to achieve maximum lift to drag ratio. It has been found that the total aerodynamic forces are sensitive to the location of the micro-cylinder. A significant enhancement of lift to drag ratio can be achieved by adding micro-cylinder in front of S809 airfoil especially at high Reynolds number.

1. Introduction

Active and passive flow controls are the two different techniques that are used to control the flow state. The active flow control is relatively restricted, as it needs an additional controller, actuators and power supply to control theflow. On the other side, passive flow control is relatively simple and cheap.Therefore, the passive flow control is more applicable in practical applications but on a narrow range of operating conditions [1,2]. Several publications investigated the impact of different passive technique on the aerodynamic performance of wind turbine blades, such as adding micro-cylinder [1,2], micro-tab [3], vertex generators, gurney flaps[4,5, 6], tubercle leading edge[7, 8, 9], split blade [10], slot [11, 12], and rod vortex generators [13]. Wang et al. 2018 discussed in detail the effect of adding micro-cylinder with different diameters and positions in front of the NREL Phase VI wind turbine blade. It was found that (1) it possibleto suppress the flow separation on wind turbine blades, (2) the blade torque was increased by 27.3%when the micro-cylinder is close to the blade leading edge point, with smaller vertical distance = $2.3\times10^{-2}$and diameter = 6.78×10^{-3} (dimensions in this paper normalized by chord). In the work of Luo et al. 2018, a micro-cylinder was added near to the leading

edge of a stalled airfoil (NACA 0012) inflow at Re= 6 x10^6;The Reynolds-averaged Navier–Stokes equations(RANS)simulations were performed to determine the optimal control parameter. Luo et al. 2018 were able to capture the transient vortical structures in the massive separation region by relying on `Delayed Detached Eddy Simulation` (DDES) for the controlled and uncontrolled cases. Overall, adding micro-cylinder improved lift coefficient and lift-to-drag ratio that can be achieved after stall. RANS and DDES results indicated that the heavy stall can be effectively delayed; the extent of large separation region, on the airfoil suction surface, can also be diminished[2].
In the currentwork, a micro-cylinder is selected as the control element and proposed to be installed around the airfoil leading edge.The S809 airfoil is chosen for simulation. This thick airfoil (21% thickness) has been designed for a horizontal axis wind turbine and tested experimentally[14]. The main objectives, that have been achieved for this airfoil comparing to the other availableairfoils, are maximizingthe lift, minimizing the profile drag, and reducing the sensitivity to roughness. Practically, the airfoil-S809 is using now for some horizontal axis wind turbine rotor;this was tested experimentally in NREL phase II (3-bladed HAWT)[15] and NREL phase VI[16] (2-bladed HAWT).This airfoil is popular for validation of numerical solutions[1, 6, 12, 17, 18].Here, the simulation will be carried out using ANSYSFluent 18.2 to investigate the impact of the location and diameter of the micro-cylinder. Response Surface Method (RSM) is employed in this simulation as the optimization tool.

This paper is organized as follows: in Section 2 the numerical approaches and governing equations are reviewed. The results are discussed in Section 3. Summary and conclusion come at the end.

2. Numerical approaches and governing equations

In this study, the simulations were carried out using ANSYSFluent 18.2 for incompressible flow. In this package, the Navier-Stokes equation is solved to resolve the fluid flow. In order to consider the turbulence effect, Reynolds-Averaged Navier-Stokes equations (RANS) andshear-stress transport (SST) k-ω turbulence model are used. These equations can be reviewed as follows:
(1) Continuity equation

$$\frac{\partial(\overline{\bar{u}_i + u_i'})}{\partial x_i} = \frac{\partial(\bar{\bar{u}}_i + \overline{u_i'})}{\partial x_i} = 0, \qquad \frac{\partial(\bar{u}_i)}{\partial x_i} = 0, \qquad \frac{\partial(\overline{u_i'})}{\partial x_i} = 0 \tag{1}$$

(2) Momentum equation

$$\frac{\partial}{\partial t}\rho(\bar{u}_i) + \frac{\partial}{\partial x_j}\rho(\bar{u}_i\bar{u}_j) = -\frac{\partial(\bar{p})}{\partial x_i} + \mu\frac{\partial}{\partial x_j}\left(\frac{\partial\bar{u}_i}{\partial x_j} - \rho\overline{(u_i'u_j')}\right) + \rho(\bar{F}_i) \tag{2}$$

In equation (1) and (2), u_j' is the turbulence fluctuation in the velocity component, $-\rho\overline{(u_i'u_j')}$term represents the product of turbulence fluctuations in the velocity components; it is known as the turbulent shear or Reynolds stresses ($\tau_{ij}' = -\rho\overline{u_i'u_j'}$) which are unknown. The Reynolds stresses cannot be calculated directly but have to be modeled. This is commonly referred to as a closure problem (See Ferziger and Peric[19]). Therefore, in 1877 the Boussines approximation was introduced, resulting in the eddy viscosity or eddy diffusion model.

$$\overline{\tau_{ij}} = \mu_t\left(\frac{\partial\bar{u}_i}{\partial x_j} + \frac{\partial\bar{u}_j}{\partial x_j}\right) - \frac{2}{3}\rho k\delta_{ij} \tag{3}$$

where μ_t is the eddy (turbulent) viscosity which has the same dimension as the molecular viscosity(μ), it isn't a fluid property but rather a turbulence property and k is the turbulent kinetic energy $k = \frac{1}{2}\left[\overline{u'}^2 + \overline{v'}^2 + \overline{w'}^2\right]$ .The problem has been transformed from one of finding the individual Reynolds stresses to one of determining the eddy (turbulent) viscosity μ_t.Shear-stress transport (SST) k-ω turbulence model is a type of hybrid model, combining two models in order to calculate flow in the near-wall region. It uses a standard k-ε model to obtain flow properties in the free-stream (turbulent) flow region far from the wall, while using a modified k-ε model near the wall using the turbulence frequency ω as a second variable instead of turbulent kinetic energy dissipation term ε, which is expressed as ω = ε/k [s^{-1}]. The transport equation for turbulent kinetic energy k for the k-ω model can be reviewed as follows[19]:

$$\frac{\partial(\rho k)}{\partial t} + \frac{\partial(\rho k \bar{u}_j)}{\partial x_j} = \frac{\partial}{\partial x_j}\left[\left(\mu + \frac{\mu_t}{\sigma_k}\right)\frac{\partial(k)}{\partial x_j}\right] + P_k - \beta^* \rho k \omega, \quad (4)$$

$$\frac{\partial(\rho \omega)}{\partial t} + \frac{\partial(\rho \omega \bar{u}_j)}{\partial x_j} = \frac{\partial}{\partial x_j}\left[\left(\mu + \frac{\mu_t}{\sigma_\omega^*}\right)\frac{\partial(\omega)}{\partial x_j}\right] + \alpha\frac{\omega}{k}P_k - \rho\beta\omega^2. \quad (5)$$

Equations [4] and [5] can be summarized as follows,

$$\begin{pmatrix}\text{Rate of change}\\ \text{of}\\ k/\omega\end{pmatrix} + \begin{pmatrix}\text{Transport of}\\ k/\omega\\ \text{by convection}\end{pmatrix} = \begin{pmatrix}\text{Transport of}\\ k/\omega\\ \text{by diffusion}\end{pmatrix} + \begin{pmatrix}\text{Rate of}\\ \text{production}\\ \text{of}\\ k/\omega\end{pmatrix} - \begin{pmatrix}\text{Rate of destruction}\\ \text{of}\\ k/\omega\end{pmatrix},$$

In this model, the eddy viscosity is expressed as $\mu_t = \rho\frac{k}{\omega}$, $\alpha = \frac{5}{9}$, $\beta = 0.075$, $\beta^* = 0.09$, $\sigma_k^* = 2$, and $\sigma_\omega^* = 2$ [14].

3. Results and discussions

In this section, the impact of adding micro-cylinder around the S809 airfoil and optimizationfor its location and diameter will be discussed.

3.1. Aerodynamic analysis around S809 using CFD

As it usual in standard computational fluid dynamic (CFD) works, the first step it to perform the mesh independent study. For that, three different meshes were examined to ensure that the simulation results are independent of grid size. Table 1 lists three different mesh sizes with the number of elements 53650, 60000, and 75254. Figure 1 shows the mesh topology and its mesh refinement around S809 airfoil. To achieve good precision the thickness of the first layer around airfoil should be $y^+<5$ and it will be more accurate if y^+approaches 1 [20].The goal is achieved by setting the first layer thickness = 2×10^{-5}m.The mesh sensitivity analysis is presented infigures.2 and 3. Where figure 2 shows the behavior of lift coefficient versus the simulation iterationat different mesh size; and figure 3 illustrate the trend of lift coefficient versus the angle of attack (AOA) at different mesh size. As it can be observed from these figures, the results become independent on the mesh size≥ 60000,therefore, so this mesh size (60000)is selectedas a default case for the current simulations. The domain dimensions at the upstream and downstream are 20 and 40 times chord length as shown in figure 1 [21].In these simulations, the boundary conditions areas follows: (1) left boundary is velocity inlet, (2) upper and lower boundaryis symmetry, (3) the right boundary is pressure outlet.In this work, the numerical approaches that have been used in the Ansys Fluent 18.2 can be summarized as follows: 1) the pressure-velocity coupling scheme (coupled), and (2) (2) Least squares (cell-based) is used for spatial discretization, (3) second-order scheme for pressure equation, (4) second-order upwind scheme for the momentum equation, and (5) second-order upwind scheme for turbulent kinetic energy and specific dissipation rate equations.

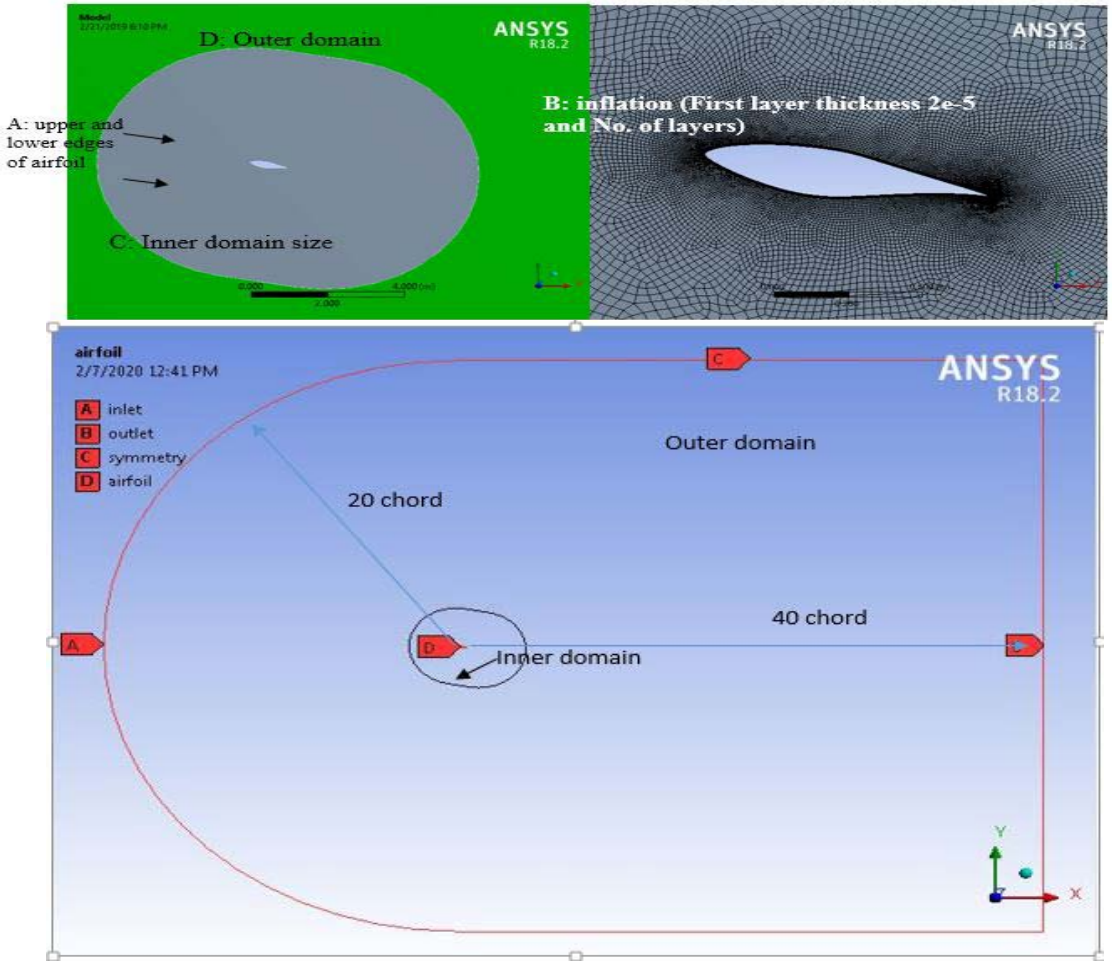

Figure 1. Mesh topology.

Table 1. Mesh Refinement.

Mesh size	A	B	C	D
53650	180	60	0.3	0.6
60000	200	70	0.3	0.6
75254	200	70	0.2	0.4

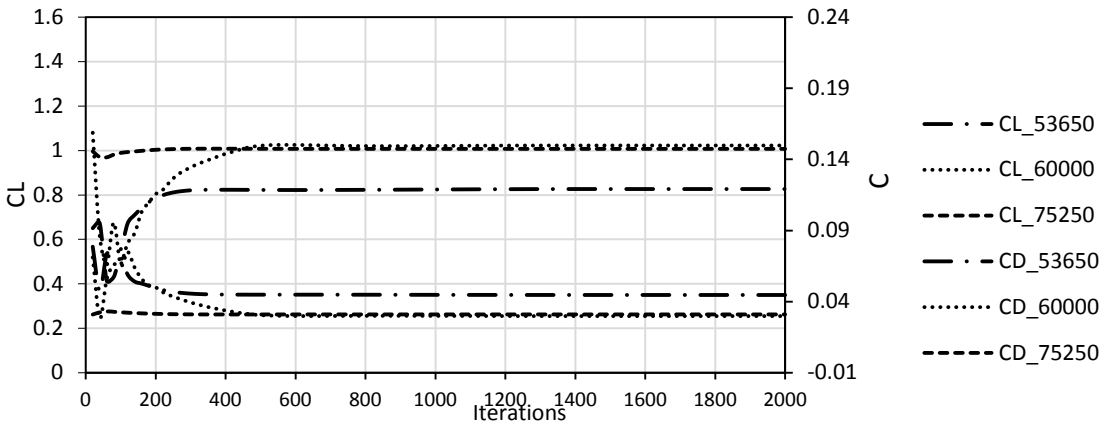

Figure 2. Lift and drag coefficient convergence history at AOA = 11.2^{o}.

Validation with experimental results [21]is performed at Reynolds number of 10^6 and Mach number of 0.044. Different angles of attacks are selected for validation, which are AOA= 0.0°, 2.1°, 4.1°, 6.1°, 8.2°, 10.1°, and 11.2°. Figure 3 shows that our numerical results for lift and drag coefficient agree well with the experimental values.

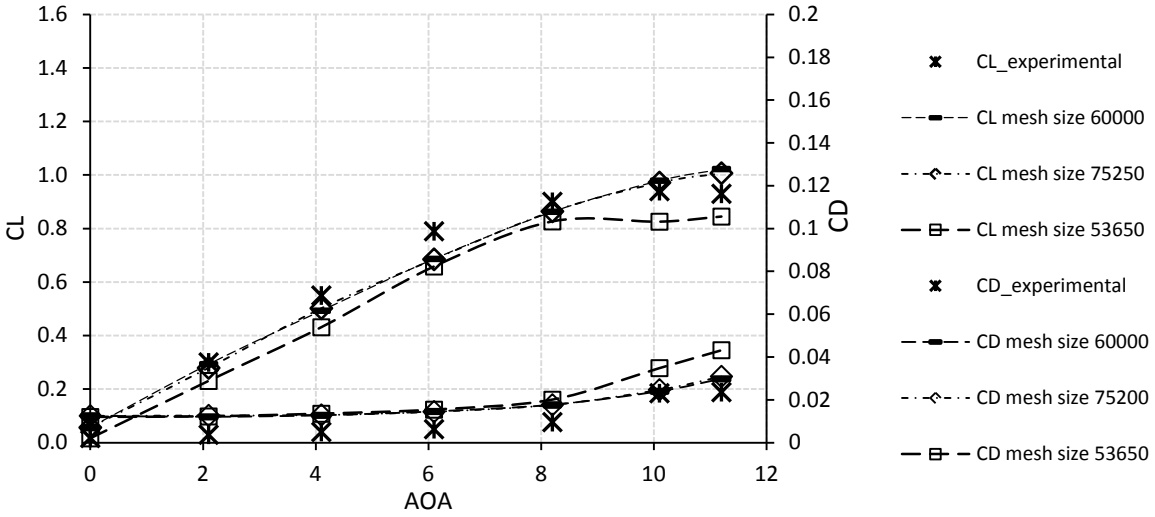

Figure 3. Lift and drag coefficient validation with experimental at $Re=10^6$.

In order to achieve our design point (The optimum location of the micro-cylinder and the optimum diameter),first the optimum angle of attack of the airfoil S809 that satisfied the target of maximum lift to drag ratio at certain design point is obtained. Thenthe optimum location and dimension of micro-cylinder at the selected design point is examined.

Response surface optimization feature impeded inANSYSpackage will be considered asthe optimization tool used in this study. Sparse grid initialization is selected to proceed the step of the Design of Experiments (DOE) which is responsible of collecting a representative set of data relating to a process, to calculate a response surface and then executing the optimizationusing Multi-Objective Genetic Algorithm (MOGA) which supports all types of input parameters.

*3.1.1.Design point analysis around S809 airfoil ($Re=7.2\times10^5$).*In this section our goal is to obtain the optimum angle of attack (AOA) at $Re=7.2\times10^5$ (corresponding velocity V=10.5 m/s). The input parameter for the optimization algorism is the angle of attack while the output parameter is the lift to drag ratio. The optimization criteria is the AOA at which maximum lift to drag ratio achieved. The maximum and minimum values of angle of attack for step of design of experiment is 0° and 14° respectively.
Design of experiment samples are illustrated in table 2, and the refinement points created by response surface are tabulated in table 3. MOGA optimization technique then applied. It has been observed that the resultant value of the optimum angle of attack that satisfied maximum lift to drag ratio is 6.65° as shown in table 4.

Table 2. Design of experiment (sparse grid initialization).

Name	P9 - AOA (degree)	P10 - cd-op	P11 - cl-op	P12 - lift-to-drag-ratio-op
1	7	0.017	0.760	45.121
2	0	0.013	0.044	3.420
3	14	0.058	0.977	16.720

Table 3. Refinement points created by response surface (sparse grid).

Name	P9 - AOA (degree)	P10 - cd-op	P11 - cl-op	P12 - lift-to-drag-ratio-op
1	3.500	0.015	0.420	28.579
2	10.500	0.029	0.961	33.487
3	8.750	0.017	0.953	55.022
4	12.250	0.041	0.990	23.914
5	7.875	0.018	0.832	46.214
6	9.625	0.023	0.937	40.429
7	1.750	0.013	0.236	17.808
8	5.250	0.015	0.595	39.355

Table 4. Optimum Lift to drag ratio after verification (MOGA).

P9 - AOA	P10 - cd-op	P11 - cl-op	P12 - lift-to-drag-ratio-op
6.65	0.016	0.722	46.412
7.77	0.018	0.823	45.849
8.85	0.020	0.899	44.321

3.2. Optimum location and diameter of micro-cylinder around S809 airfoil (Re=720000)

From the previous section, the optimum angle of attack that satisfied maximum lift to drag ratio is calculated. Then the next step is to optimize the micro-cylinder location and diameter as it will be discussed in the next section. The following study focus mainly on two positions of the micro cylinder: (1) micro-cylinder is just above the upper surface of the airfoil, and (2) micro-cylinder is front of the S809 airfoil leading edge. In the following section the general setting of micro-cylinder will be illustrated.

3.2.1. General setting for different optimization methods. As the first test, the micro-cylinder is added and the number of cells = 66824 cell, AOA = 6.65^{o}(optimum one)corresponding to wind speed = 10.5 m/s as shown in table 4 and figure 4. The input parameters are (1) dx which is the horizontal distance between micro-cylinder and blade leading edge, (2) dy which isthe vertical distance between micro-cylinder and blade leading edge, and (3) D which is the diameter of cylinder all dimensions are normalized by chord length in this paper chord length = 1m . The output parameters are (1) lift and drag coefficients, and (2) lift to drag ratio. The optimization technique is response surface optimization method as stated before. In this optimization, Latin hypercube sampling design is chosen for Design of Experiments (DOE); Response Surface method is Kriging; and optimization technique is MOGA.

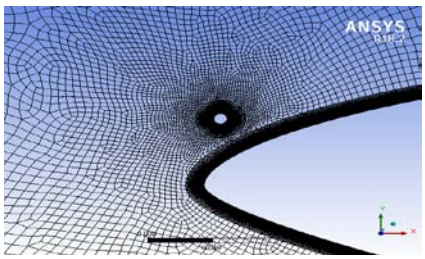

Figure 4. Grid topology around airfoil with micro-cylinder.

3.2.2.Optimization of micro cylinder location above the upper surface of S809 airfoil. In this section, micro-cylinder is located above the upper surface of the S809 airfoil to illustrate the effect of adding it on the values of lift to drag ratio. The range of horizontal distance from leading edge is dx=0 - 0.05, vertical distances from leading edge of the airfoil is dy = 0.054 - 0.08 and diameter of micro-cylinder is D = 0.008 - 0.02 as illustrate in figure 5.

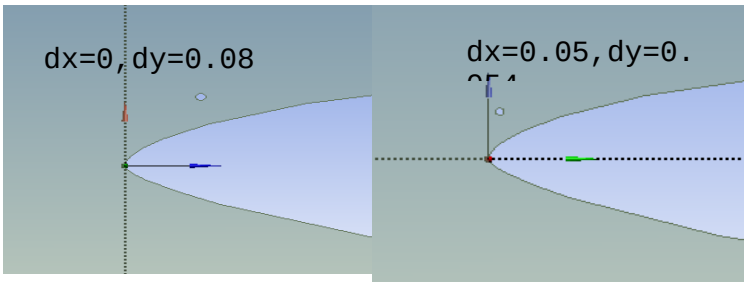

Figure 5. Samples of addingthe micro-cylinder above upper surface of airfoil.

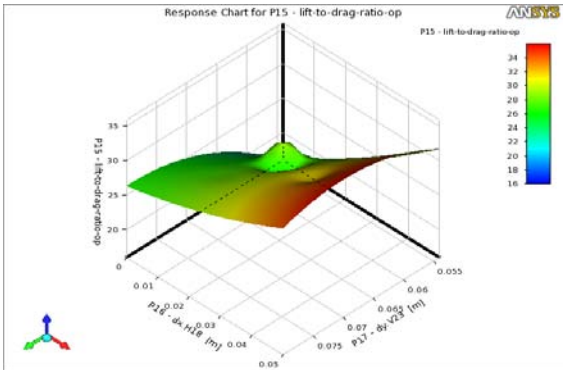

Figure 6..Response chart of lift to drag ratio versus dx and dy.

Kriging method is selected to create the response surface as shown in figure 6. This method is non-parametric, meaning that the prediction will depend on all existing data points. Thus the method could be slow in case of usinglarge amount of data. It is also slow in fitting the data due to the calculation of pair-wise distances among data points. However, this method automatically fits through all data points.

By using MOGA optimizationmethod, the location of micro-cylinder with AOA =6.65 found to be at dx = 0.05, dy = 0.056, and D = 0.008.

*3.2.3 Off-design charts in case of existence of micro-cylinder above upper surface.*At optimized location of micro-cylinder off design charts was created to predict the flow behavior. The variation of the lift coefficient, drag coefficient, and the lift to drag ratio versus angle of attack with and without the micro-cylinder are shown in figures 7, 8, and 9 respectively.

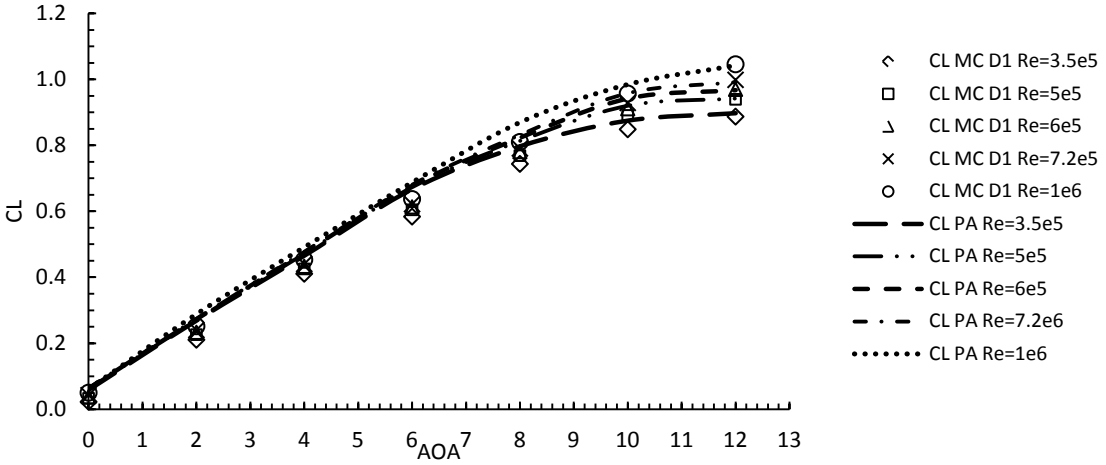

Figure 7. Lift coefficient versus AOA. Lines representairfoilwithout the micro-cylinder. Symbols are used to represent the cases with adding the micro-cylinder.

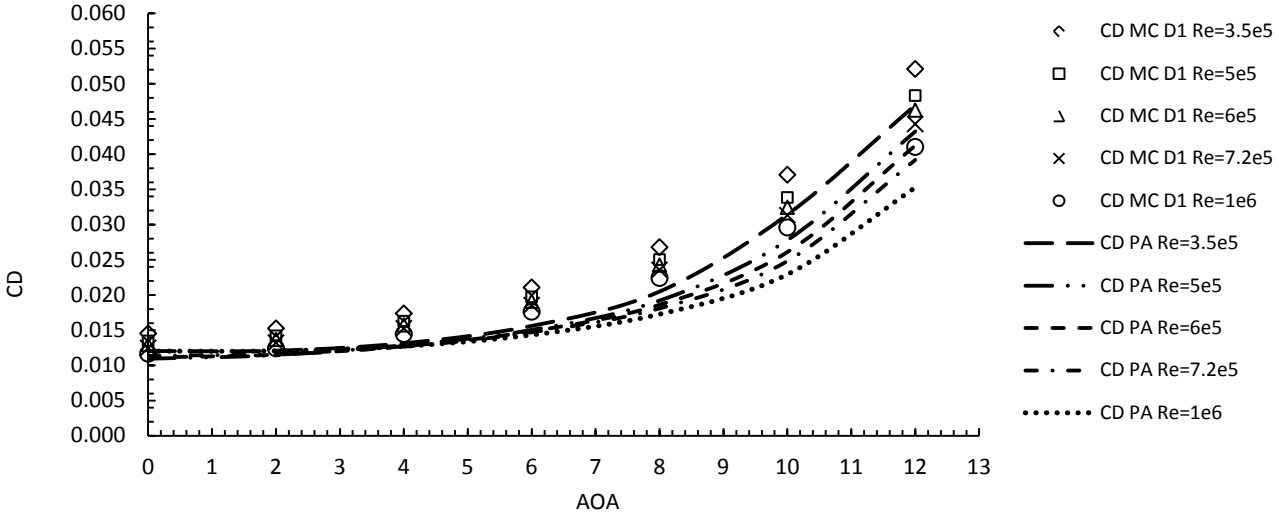

Figure 8. Drag coefficient versus AOA.Lines representairfoilwithout the micro-cylinder. Symbols are used to represent the cases with adding the micro-cylinder.

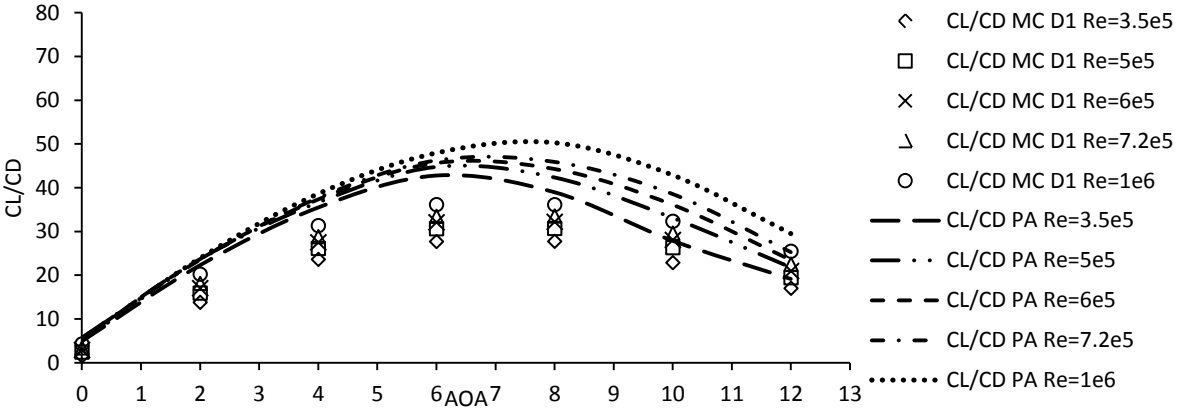

Figure 9. Lift to drag ratio versus AOA. Lines representairfoilwithout the micro-cylinder. Symbols are used to represent the cases with adding the micro-cylinder.

It is clear from these figures (7, 8, and 9) thatadding the micro-cylinder above the upper surface of S809 airfoil, slightly decreases the lift coefficient as shown in figure 7 while the drag coefficient is increased as shown in figure 8.Consequently, the lift to drag ratio is decreased as shown in figure 9. So it is concluded that the adding the micro-cylinder above upper surface of the airfoil will affect negatively on the aerodynamic performance.

3.2.4 Optimization of micro cylinder location in front of the S809 airfoil leading edge. The micro-cylinder now is located in front of the S809 airfoil leading edge to examine the impact on the values of lift to drag ratio. The range of horizontal dx = 0.01-0.06, and vertical distances dy = 0 - 0.06 , from leading edge of the airfoil and diameter of micro-cylinder D = 0.002 – 0.02 , examples of distances are illustrate in figure10.

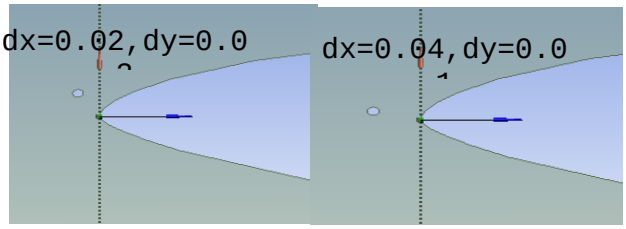

Figure 10. Samples of addingthe micro-cylinder in front of the S809 airfoil leading edge.

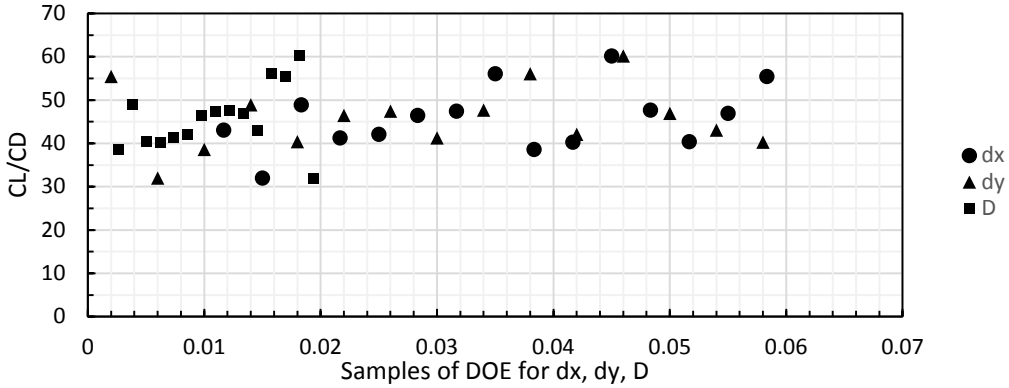

Figure 11. Lift to drag ratio versus input parameters (Design of experiments LHS).

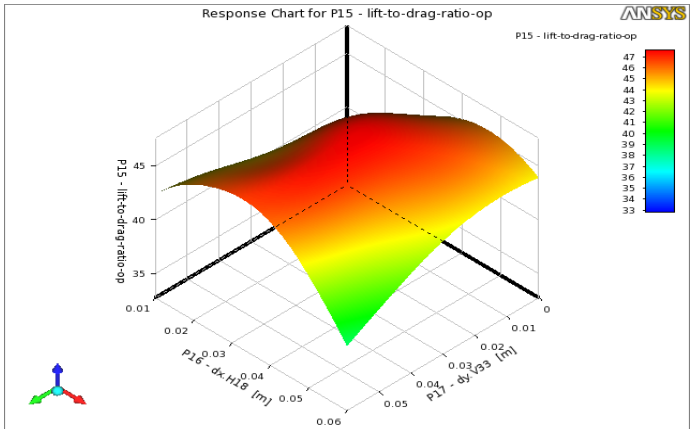

Figure 12. Response chart of Lift to drag ratio versus dx and dy.

Latin hypercube sampling design are shown in figure 11 and the created response Surface is shown in figure 12.It has been observed that the values of lift to drag ratio in figure 12 are greater than that

infigure 6 (case with adding the micro-cylinder above the airfoil). From MOGA optimization tool it is found that the optimum location is dx = 0.05, dy = 0.05, D = 0.02.

*3.2.5.Off-design Charts in case of existence of micro-cylinder in front of the S809 airfoil leading edge.*It is clear from the above figures (11- 14) thatwhen adding micro-cylinder in front of the S809 airfoil leading edge, the lift coefficient is slightly decreased as shown in figure 13 while the drag coefficient is highly decreased as shown in figure 14. As a consequence, the lift to drag ratio is increased as shown in figure 15. Therefore, it can be concluded that the adding of micro-cylinder in front of the S809 airfoil leading edge will affect positively on the values of lift to drag ratio and consequently the aerodynamic performance.

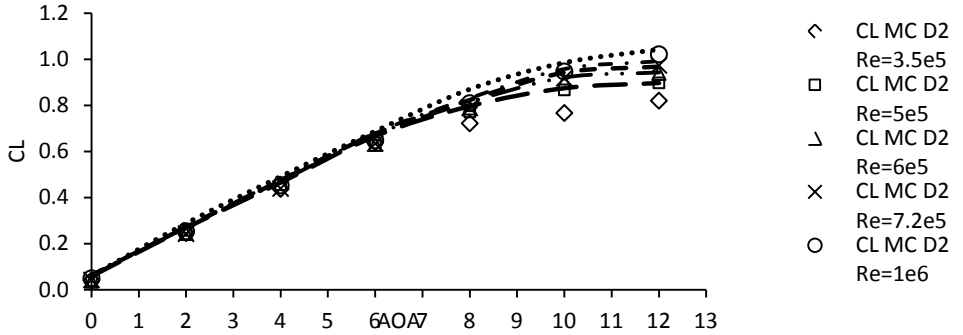

Figure 13. Lift coefficient versus AOA .Lines representairfoilwithout the micro-cylinder. Symbols are used to represent the cases with adding the micro-cylinder.

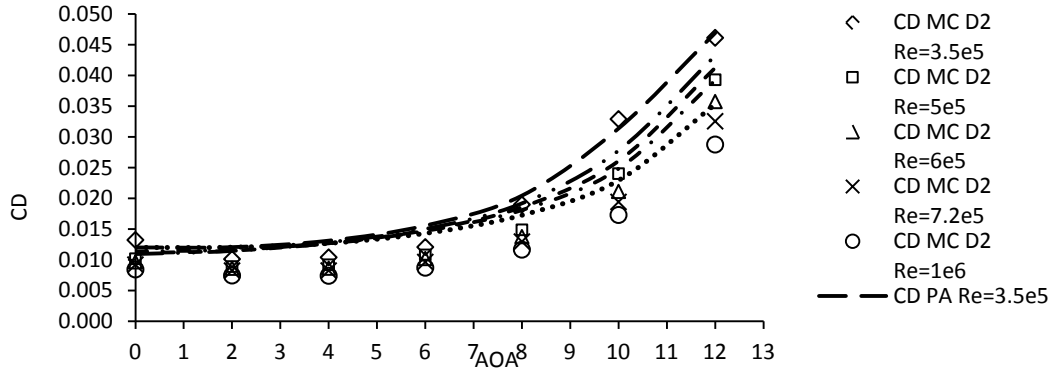

Figure 14. Drag coefficient versus AOA. Lines representairfoilwithout the micro-cylinder. Symbolsare used to represent the cases with adding the micro-cylinder.

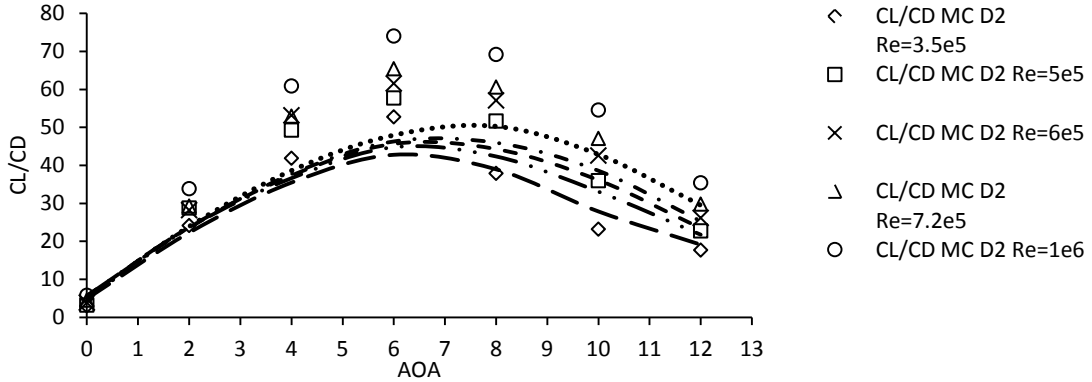

Figure 15. Lift to drag ratio versus AOA. Lines representairfoilwithout the micro-cylinder. Symbols are used to represent the cases with adding the micro-cylinder.

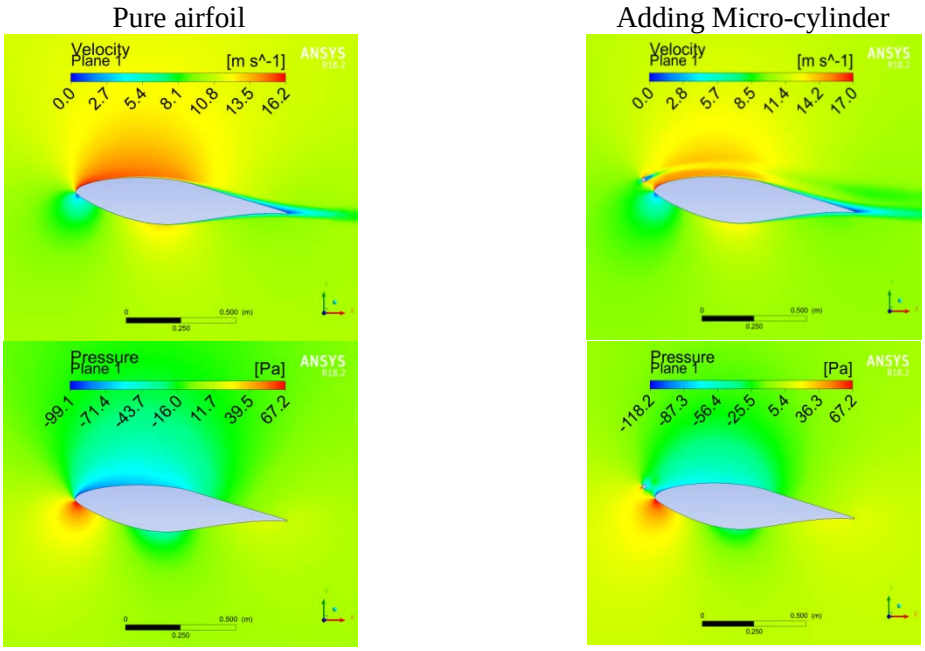

Figure 16. Comparison of the velocity distribution and pressure distribution respectively around the controlled and uncontrolled S809 airfoils at angle of attack 6.1^{o}

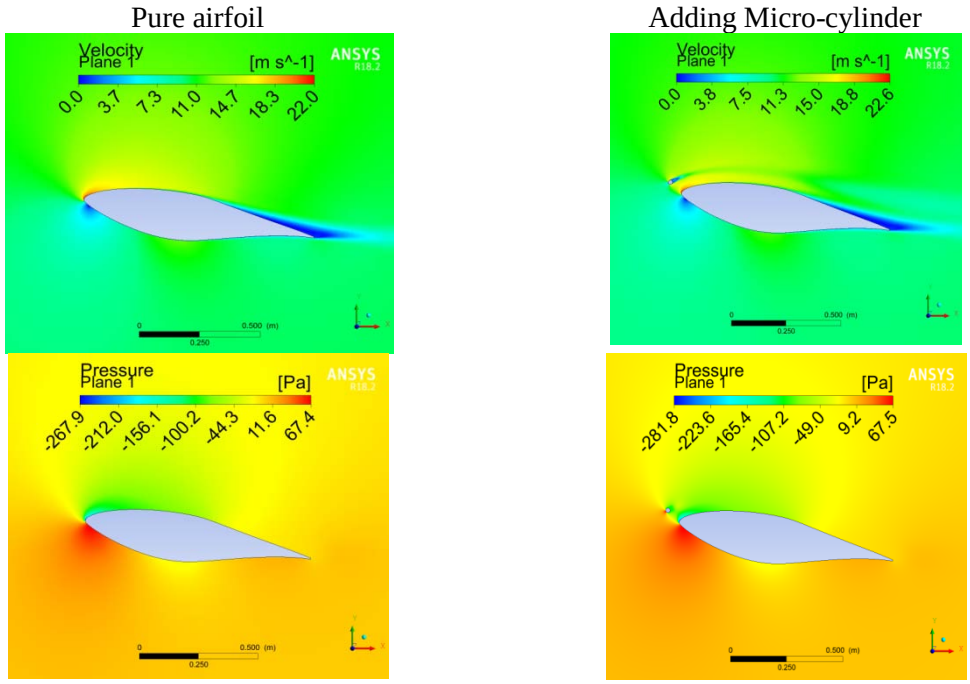

Figure 17. Comparison of the velocity distribution and pressure distribution respectively around the controlled and uncontrolled S809 airfoils at angle of attack 10.1^{0}.

The presence of the micro-cylinder affects the velocity and pressure distribution around the S809 airfoil,the change in velocity and pressure distribution at the angle of attack 6.1^{o} is greater than that at the angle of attack 10.1^{o} as shown in figures 16 and 17. These agree with the results are shown in figure 15, where the values of lift to drag ratio has a peak value at angles of attack around

6.65^{o}.Therefore, the micro-cylinder has a direct impact on the total aerodynamic forces and leads to a decrease in the drag coefficient and highly increase in the lift to drag ratio as shown in figures 14, 15.

4. Conclusion

A passive flow control strategy for the S809airfoil was investigated inthis study. The effect of installing a micro-cylinder near the S809 airfoil was numerically investigated, with a focus on thetotal aerodynamic forces and flow fields at angle of attacks ranging from 0 to 12 .Thediameter and the location of the micro-cylinder were theinput parametersto be considered in this investigation and lift to drag ratio was the output parameter. Response surface optimization tool was the method used to calculate the input parameter and achieving the target of maximum lift to drag ratio. The main results from this study is that adding micro-cylinder in front of the leading edge increases the lift to drag ratio especially at Reynolds numbers above $5\times10^5$and angles of attack from 4^0 to 10^0, while the effect is slightly less at low velocities, Re = 3.5×10^5 .

Reference

[1] Wang Y, Li G, Shen S, Huang D and Zheng Z 2018 Investigation on aerodynamic performance of horizontal axis wind turbine by setting micro-cylinder in front of the blade leading edge. *Energy*, **143**, pp.1107-1124

[2] Luo D, Huang D and Sun X 2017 Passive flow control of a stalled airfoil using a microcylinder. *Journal of Wind Engineering and Industrial Aerodynamics*, **170**, pp.256-273.

[3] Ebrahimi A and Movahhedi M 2018. Wind turbine power improvement utilizing passive flow control with microtab. *Energy*, **150**, pp.575-582

[4] Fernandez-Gamiz U, Zulueta E, Boyano A, Ansoategui I and Uriarte I 2017Five megawatt wind turbine power output improvements by passive flow control devices. *Energies*, **10(6)**, p.742

[5] Holst D, Pechlivanoglou G, Wegner F, Nayeri C N and Paschereit C O 2017Potential of Retrofit Passive Flow Control for Small Horizontal Axis Wind Turbines. *Journal of Engineering for Gas Turbines and Power*, **139(3)**, pp.1-8

[6] Wang H, Zhang B, Qiu Q and Xu X 2017 Flow control on the NREL S809 wind turbine airfoil using vortex generators. *Energy*, **118**, pp.1210-1221

[7] Aftab S M A and Ahmad K A 2017 CFD study on NACA 4415 airfoil implementing spherical and sinusoidal Tubercle Leading Edge. *PloS one*, **12(11)**,pp.1-27

[8] Asli M, Mashhadi Gholamali B and Mesgarpour Tousi A 2015 Numerical analysis of wind turbine airfoil aerodynamic performance with leading edge bump. *Mathematical Problems in Engineering*, **2015**

[9] Huang G Y, Shiah Y C, Bai C J and Chong W T 2015 Experimental study of the protuberance effect on the blade performance of a small horizontal axis wind turbine. *Journal of Wind Engineering and Industrial Aerodynamics*, **147**, pp.202-211

[10] Moshfeghi M, Shams S and Hur N 2017Aerodynamic performance enhancement analysis of horizontal axis wind turbines using a passive flow control method via split blade. *Journal of Wind Engineering and Industrial Aerodynamics*, **167**, pp.148-159

[11] Semwal M, Tripathi R, Sati N, Rana V and Rawat K S 2016 Drag reduction of wind turbine blade to enhance aerodynamic performance: A numerical study. *International Journal of Scientific & Engineering Research*,**7(12)**, pp. 199–203

[12] Xie Y, Chen J, Qu H, Xie G, Zhang D and Moshfeghi M 2013 Numerical and experimental investigation on the flow separation control of S809 airfoil with slot. *Mathematical Problems in Engineering*, **2013**

[13] Ostachowicz W, McGugan M, Schröder-Hinrichs J U and Luczak M eds2016 *MARE-WINT: new materials and reliability in offshore wind turbine technology*. Springer.

[14] Somers D M 1997 *Design and experimental results for the S809 airfoil* (No. NREL/SR-440-6918). National Renewable Energy Lab., Golden, CO (United States).

[15] Butterfield C P, Musial W P, Scott G N and Simms D A 1992 *NREL Combined Experimental Final Report--Phase II* (No. NREL/TP-442-4807). National Renewable Energy Lab.(NREL), Golden, CO (United States).
[16] Lindenburg C 2003*Investigation into Rotor Blade Aerodynamics Analysis of the stationary measurements on the UAE phase-VI rotor in the NASA-Ames wind tunnel*. Energy research Centre of the Netherlands (ECN) Wind Energy publication, ECN-C--03-025.
[17] Moshfeghi M, Song Y J and Xie Y H 2012Effects of near-wall grid spacing on SST-K-ω model using NREL Phase VI horizontal axis wind turbine. *Journal of Wind Engineering and Industrial Aerodynamics*, **107**, pp.94-105
[18] Wang Y, Zheng X, Hu R and Wang P 2016 Effects of Leading Edge Defect on the Aerodynamic and Flow Characteristics of an S809 Airfoil. *PloS one*, **11(9)**, pp. 1-17
[19] Ferziger J H and Peric M 2002*Computational Methods for Fluid Dynamics*Third, Rev Edition, Springer, 2002.
[20] El Khchine Y and Sriti M 2017 Boundary Layer and Amplified Grid Effects on Aerodynamic Performances of S809 Airfoil for Horizontal Axis Wind Turbine (HAWT). *Journal of Engineering Science & Technology*, **12(11)**, pp.3011-3022
[21] He Y and Agarwal R K 2014 Shape optimization of NREL S809 airfoil for wind turbine blades using a multiobjective genetic algorithm. *International Journal of Aerospace Engineering*, **2014**

Appendix : TableA. Coordinates and characteristics of NREL airfoil

X/C	Y/C	X/C	Y/C	X/C	Y/C
1	0	0.171409	0.078687	0.193738	-0.08357
0.996203	0.000487	0.136174	0.07058	0.231914	-0.09244
0.98519	0.002373	0.104263	0.061697	0.271438	-0.09991
0.967844	0.00596	0.076035	0.052224	0.311968	-0.10528
0.945073	0.011024	0.051823	0.042352	0.35337	-0.10818
0.917488	0.017033	0.03191	0.032299	0.395329	-0.10801
0.885293	0.023458	0.01659	0.02229	0.438273	-0.10455
0.848455	0.03028	0.006026	0.012615	0.48192	-0.09735
0.80747	0.037766	0.000658	0.003723	0.527928	-0.08657
0.763042	0.045974	0.000204	0.001942	0.576211	-0.07398
0.715952	0.054872	0	-0.00002	0.626092	-0.06064
0.667064	0.064353	0.000213	-0.00179	0.676744	-0.04744
0.617331	0.074214	0.001045	-0.00348	0.727211	-0.0351
0.56783	0.084095	0.001208	-0.00372	0.776432	-0.0242
0.519832	0.093268	0.002398	-0.00527	0.823285	-0.01516
0.474243	0.099392	0.009313	-0.0115	0.86663	-0.0082
0.428461	0.10176	0.02323	-0.0204	0.905365	-0.00336
0.382612	0.10184	0.04232	-0.03027	0.938474	-0.00049
0.33726	0.10007	0.065877	-0.04082	0.965086	0.000743
0.29297	0.096703	0.093426	-0.05192	0.984478	0.000775
0.250247	0.091908	0.124111	-0.06308	0.996141	0.00029
0.209576	0.085851	0.157653	-0.07373	1	0